Characterization of Neuroblastic Tumors Using ^{18}F-FDOPA PET

Meng-Yao Lu*[1], Yen-Lin Liu*[2,3], Hsiu-Hao Chang[1], Shiann-Tarng Jou[1], Yung-Li Yang[1], Kai-Hsin Lin[1], Dong-Tsamn Lin[1], Ya-Ling Lee[4], Hsinyu Lee[5,6], Pei-Yi Wu[5], Tsai-Yueh Luo[7], Lie-Hang Shen[7], Shiu-Feng Huang[8], Yung-Feng Liao[9], Wen-Ming Hsu[10], and Kai-Yuan Tzen[11], for the National Taiwan University Neuroblastoma Study Group

[1]Department of Pediatrics, National Taiwan University Hospital, Taipei, Taiwan; [2]Degree Program of Translational Medicine, Academia Sinica–National Taiwan University, Taipei, Taiwan; [3]Department of Pediatrics, Buddhist Tzu Chi General Hospital, Taipei Branch, New Taipei, Taiwan; [4]Department of Nursing, National Taiwan University College of Medicine, Taipei, Taiwan; [5]Institute of Zoology, National Taiwan University College of Life Science, Taipei, Taiwan; [6]Department of Life Science, National Taiwan University College of Life Science, Taipei, Taiwan; [7]Institute of Nuclear Energy Research, Taoyuan, Taiwan; [8]Institute of Molecular and Genomic Medicine, National Health Research Institute, Miaoli, Taiwan; [9]Institute of Cellular and Organismic Biology, Academia Sinica, Taipei, Taiwan; [10]Department of Surgery, National Taiwan University Hospital, Taipei, Taiwan; and [11]Department of Nuclear Medicine, National Taiwan University Hospital, Taipei, Taiwan

Neuroblastic tumors are childhood neoplasms that possess amino acid decarboxylase (AADC) activity and can theoretically be imaged by ^{18}F-fluorodihydroxyphenylalanine (^{18}F-FDOPA) PET, a new diagnostic tool for neuroendocrine tumors. In this study, we explored the accuracy and clinical role of ^{18}F-FDOPA PET in neuroblastic tumors. **Methods:** From 2008 to 2011, patients with tissue-proven neuroblastic tumors receiving ^{18}F-FDOPA PET at initial diagnosis or during follow-ups were enrolled. The sensitivity and specificity of ^{18}F-FDOPA PET were compared with those of ^{123}I-metaiodobenzylguanidine (^{123}I-MIBG) scintigraphy and ^{18}F-FDG PET, using tumor histology as the standard. The maximum standardized uptake value and tumor-to-liver uptake ratio on ^{18}F-FDOPA PET were measured and correlated with AADC messenger RNA level in tumor tissue. **Results:** Fifty tumors from 34 patients, including 42 neuroblastic tumors and 8 lesions without viable tumor cells, were eligible for analysis. ^{18}F-FDOPA PET successfully detected neuroblastic tumors of different histologic types in various anatomic sites, at a sensitivity of 97.6% (87.4%–99.9%) and a specificity of 87.5% (47.3%–99.7%). In tumors with concomitant studies, ^{18}F-FDOPA PET demonstrated a higher sensitivity than ^{123}I-MIBG scintigraphy ($n = 18$; $P = 0.0455$) or ^{18}F-FDG PET ($n = 46$; $P = 0.0455$). Among the 18 tumors with concomitant ^{123}I-MIBG scans, 4 tumors with viable cells were ^{123}I-MIBG–negative but were successfully detected by ^{18}F-FDOPA PET. The tumor uptake of ^{18}F-FDOPA significantly correlated with AADC expression ($n = 15$ nonhepatic tumors; maximum standardized uptake value, $P = 0.0002$; tumor-to-liver uptake ratio, $P < 0.0001$). **Conclusion:** ^{18}F-FDOPA PET showed high sensitivity and specificity in detecting and tracking neuroblastic tumors in this preliminary study with a small cohort of patients and might be complementary to ^{123}I-MIBG scintigraphy and ^{18}F-FDG PET. By correlating with AADC expression, ^{18}F-FDOPA PET might serve as a useful imaging tool for the functional assessment of neuroblastic tumors.

Key Words: neuroblastoma; ganglioneuroma; ^{18}F-FDOPA; positron emission tomography; sensitivity and specificity

J Nucl Med 2013; 54:42–49
DOI: 10.2967/jnumed.112.102772

Neuroblastic tumors are the most common extracranial neoplasms in children and usually lead to a lethal result (*1*). Neuroblastic tumors are derived from precursors of the sympathetic nervous system (*2*) and secrete catecholamines or their metabolites (*3*). The primary tumors frequently arise from the adrenal glands or paraspinal ganglia in the retroperitoneum, or sometimes from the mediastinum, neck, and pelvis. Substantial metastatic diseases in the bone, bone marrow, lymph nodes, or liver may also be present at diagnosis (*4*). Therefore, the assessment of neuroblastic tumors requires a multitude of studies, including anatomic imaging (CT or MR), histologic examination of primary or metastatic tumors, bone marrow studies, and evaluation of urinary catecholamine levels (*5*). To detect viable neuroblastic cells noninvasively, functional scans, such as ^{131}I-/^{123}I-metaiodobenzylguanidine (^{131}I-/^{123}I-MIBG) scintigraphy, ^{99m}Tc-methylene diphosphonate bone scanning, and ^{18}F-FDG PET, have been performed with variable sensitivity and specificity (*5*).

By targeting the catecholamine biosynthesis pathway, 6-^{18}F-fluoro-L-dihydroxyphenylalanine (^{18}F-FDOPA) PET has been used in visualizing neuroendocrine tumors, such as pheochromocytoma, paraganglioma, gastroenteropancreatic

Received Jan. 21, 2012; revision accepted Jul. 27, 2012.
For correspondence or reprints contact either of the following: Kai-Yuan Tzen, Department of Nuclear Medicine, National Taiwan University Hospital, 7 Chung Shan S. Rd., Taipei 10002, Taiwan.
E-mail: tzenky@ntuh.gov.tw
Wen-Ming Hsu, Department of Surgery, National Taiwan University Hospital, 7 Chung Shan S. Rd., Taipei 10002, Taiwan.
E-mail: billwmhsu@gmail.com
*Contributed equally to this work.
Published online Dec. 4, 2012.

neuroendocrine tumors, and medullary thyroid carcinoma (*6,7*). ^{18}F-FDOPA resembles natural L-DOPA, which competes with large neutral amino acids in the plasma and is transported into the neurons by various amino acid transporters (*8*). The short-term accumulation of ^{18}F-FDOPA in neurons is determined mainly by the reaction rate of amino acid decarboxylase (AADC; encoded by the *DDC* gene on chromosome 7p12.2), which converts ^{18}F-FDOPA to ^{18}F-fluorodopamine, which is then stored in vesicles. Because the physical half-life of ^{18}F is 110 min, PET recordings show the total radioactivity concentration in living tissue, irrespective of any biotransformation of the tracer (*9*). In neuroendocrine tumors, the increased transport and AADC activity result in intracellular retention of metabolized ^{18}F-FDOPA and positive signals on PET images (*10,11*). In neuroblastic tumors, the neuroblastic cells also possess AADC activity (*12*) and, thus, theoretically can also be imaged by ^{18}F-FDOPA PET.

The aim of this study was to characterize the imaging features and to examine the accuracy of ^{18}F-FDOPA PET in neuroblastic tumors, using tumor histology as the gold standard. The diagnostic performance of ^{18}F-FDOPA PET was compared with those of ^{18}F-FDG PET and ^{123}I-MIBG scanning in patients with concomitant studies. Furthermore, we tested the hypothesis that ^{18}F-FDOPA uptake of neuroblastic tumors corresponds to AADC gene expression and catecholamine metabolism.

MATERIALS AND METHODS

Patients

From August 2008 to August 2011, we recruited patients diagnosed with neuroblastic tumors for serial ^{18}F-FDOPA, ^{18}F-FDG, and ^{123}I-MIBG scans before therapy and during follow-ups at National Taiwan University Hospital. When there was a clinical diagnosis of neuroblastic tumors, we arranged for functional imaging studies as well as standard clinical evaluations, including CT/MR imaging, urinary vanillylmandelic acid (VMA) level, and bone marrow smear and biopsy, followed by tumor biopsy or resection. The scans were obtained before treatment and at an interval of 3–12 mo during and after treatment. The findings were interpreted as positive or negative by an experienced nuclear medicine physician who was masked to the clinicopathological backgrounds of patients. The method of operation was decided by the pediatric surgeon, based on preoperative anatomic imaging, the resectability of the tumor, and the patient's clinical condition. Whenever possible, total resection was the first consideration. However, when the main tumor encapsulated major organs, great vessels, or nerves, a biopsy was taken from a part of the tumor with the safest accessibility, to minimize harm to the patient. Only neuroblastic tumor patients with concomitant ^{18}F-FDOPA imaging and tumor histology were included in this analysis.

The histologic classification of neuroblastic tumors was based on the International Neuroblastoma Pathology Classification (*13*). The tumor status of *MYCN* amplification was evaluated using chromogenic in situ hybridization analysis (*14*). All patients were staged according to the International Neuroblastoma Staging System (*15*). Patients were treated with surgery alone or a combination of multiple modalities including chemotherapy, radiotherapy, or autologous hematopoietic stem cell transplantation and 13-*cis*-retinoic acid according to their risk grouping (*16,17*). The treatment response was observed in accordance with the International Neuroblastoma Response Criteria (*15*). Urinary VMA level was measured from 12- or 24-h urine collections, assayed by high-performance liquid chromatography (Bio-Rad Laboratories), and reported as mg/d. The study was approved by National Taiwan University Hospital Research Ethics Committee, and informed consent was obtained from each participant's guardian.

Production of ^{18}F-FDOPA

^{18}F-FDOPA was produced in-house with a commercial automatic synthesis system (TRACERlab FX_{FE}; GE Healthcare) (*18*). Briefly, ^{18}F-fluorine was produced in the National Taiwan University Hospital PETtrace cyclotron and then reacted with the protected trimethylstannyl precursor (*N*-formyl-3,4-di-tert-butoxycarbonyloxy-6-[trimethylstannyl]-L-phenylalanine ethyl ester; ABX) in Freon (DuPont) at 5°C. A deprotection step was performed with HBr and then neutralization with NH_4OH. The product was purified with semipreparative high-performance liquid chromatography followed by sterile filtration. After a series of quality control procedures, the ^{18}F-FDOPA–containing product solution was ready for intravenous injection. The radiochemical yield of ^{18}F-FDOPA was 20%–30% (decay-uncorrected) in a synthesis time of 50–60 min from the end of bombardment. The radiochemical purity was greater than 95%, and the specific activity was greater than 222 kBq/μg.

Image Acquisition and Data Analysis

All nuclear medicine scans were obtained in random order among one another within the same admission, depending on the production schedule of the radiopharmaceuticals. All images were acquired in 2 dimensions according to the standard procedures described below. We performed a routine sedation 30 min before scanning if necessary.

For ^{18}F-FDOPA imaging, patients were pretreated with a 2 mg/kg dose of carbidopa orally an hour before injection of ^{18}F-FDOPA (*19–21*). Whole-body PET/CT images were acquired 90 min after injection of ^{18}F-FDOPA (4 MBq/kg) on a PET/CT scanner with low-amperage CT (Discovery ST-16; GE Healthcare). Whole-body ^{18}F-DOPA PET acquisitions included 5–9 bed positions (5 min per bed position) and were reconstructed using an iterative algorithm. Nondiagnostic CT (low-amperage CT with 140 kV, 40–80 mA, 0.5 s/rotation) was used for attenuation correction and for anatomic localization of the hot spots of the PET study.

Before the ^{18}F-FDG PET/CT study, patients were instructed to fast for at least 4 h. ^{18}F-FDG (5 MBq/kg) supplied by the PET Center of National Taiwan University Hospital was administered intravenously in an infusion line connected to saline. The same PET/CT scanner was used for imaging, with low-amperage CT at the same setting acquired first, followed by the PET acquisition (4 min per bed position) 45–60 min after ^{18}F-FDG injection.

For the ^{18}F-FDOPA and ^{18}F-FDG PET images, the maximum standardized uptake value (SUV_{max}) was determined for the lesion using elliptic regions of interest manually drawn around areas of abnormal uptake as delineated on the PET/CT image. SUV_{max} was chosen because of its lower sensitivity to partial-volume effects and higher reproducibility between observers. A region of interest large enough to cover more than half the lesion was used, avoiding

peripheral areas of the lesion to prevent the partial-volume effect. SUV_{max} measurements from the liver were obtained in a similar fashion. The regions of interest in the liver were free of visible metastatic disease and showed homogeneous signal intensity as delineated on the PET/CT image. All SUV_{max} calculations were performed on the transaxial attenuation-corrected PET slices. SUV_{max} corrected for lean body mass was automatically generated with software from GE Medical Systems on a Xeleris 2 workstation (GE Healthcare). Activity counts in the regions of interest were normalized to injected doses per kilogram of patient body weight. To be more objective, we also calculated the tumor-to-liver SUV_{max} ratio.

^{123}I-MIBG was produced by the Institute of Nuclear Energy Research (Taoyuan, Taiwan) (*22*) and was injected intravenously with an administered activity of 7.4 MBq/kg (80–370 MBq) on the third day of a 3-d course of Lugol solution. Anterior and posterior whole-body ^{123}I-MIBG scans were acquired 24 h after tracer injection. The dual-head γ-camera (Infinia Hawkeye; GE Healthcare) equipped with low-energy high-resolution parallel-hole collimators was used for scanning. The scanning speed for whole-body imaging was 8 min/step/30 cm in step-and-shoot mode. SPECT images were obtained for some patients in specific sections of the body, according to the clinical history of the patient and tumor localization (e.g., thorax or abdomen). For SPECT acquisition, the following parameters were used: 60 projections, a 128 × 128 matrix, and a 60-s acquisition time per projection. The data were reconstructed by standard filtered backprojection using a Butterworth filter.

Real-Time Polymerase Chain Reaction Analysis of AADC

AADC messenger RNA expression levels were analyzed by real-time polymerase chain reaction (*23*). Only nonhepatic tumors with sufficient samples were included because of endogenous expression of AADC in liver. Briefly, fresh tumor tissue was obtained during the patients' routine surgical treatment and immediately cryopreserved in liquid nitrogen, and total RNA was later extracted using TRIzol reagent (Invitrogen) and converted to complementary DNA by reverse transcriptase (SuperScript II; Invitrogen). Real-time polymerase chain reaction was performed using the iCycler iQ Real-Time PCR Detection System (Bio-Rad). A primer set of 5′-GAACAGACTTAACGGGAGCCTTT-3′ (forward) and 5′-AATGCCGGTAGTCAGTGATAAGC-3′ (reverse) was used to detect 2 AADC messenger RNA isoforms that have been reported in various neuroblastoma cell lines (*24,25*). The primer set for glyceraldehyde-3-phosphate dehydrogenase was 5′-GTGGTCTCCTCTGACTTCAAC-3′ (forward) and 5′-TCTCTTCCTCTTGTGCTCTTG-3′ (reverse). The cycling condition was 95°C for 1.5 min, followed by 40 cycles of 95°C for 30 s, 60°C for 30 s, and 72°C for 30 s. For quantification, the AADC messenger RNA expression level was normalized to that of glyceraldehyde-3-phosphate dehydrogenase. The results from 3 separate experiments were averaged.

Statistical Analysis

The sensitivity and specificity of ^{18}F-FDOPA PET, ^{18}F-FDG PET, and ^{123}I-MIBG scans with 95% confidence intervals were calculated using tumor histology as the gold standard and compared using the McNemar test. Receiver-operating-characteristic analysis was performed for ^{18}F-FDOPA and ^{18}F-FDG PET. The association between tumor uptake of ^{18}F-FDOPA and AADC messenger RNA or urinary VMA levels was evaluated by the Spearman nonparametric correlation test. Numeric data between groups were compared using the Wilcoxon rank-sum test. The statistical analyses were performed with Small Stata 11.0 software (StataCorp). All tests were 2-sided, and those with a P value of 0.05 or less were considered statistically significant.

RESULTS

Clinical Features of Patients and Tumors

During the studied period, 55 patients were enrolled and 80 scan were performed using ^{123}I-MIBG scintigraphy, 202 using ^{18}F-FDOPA PET, and 205 using ^{18}F-FDG PET. The imaging procedures were well tolerated. Thirty-four patients with 50 tumors with concomitant tissue histology and ^{18}F-FDOPA PET scans were eligible for analysis. There were 20 boys and 14 girls, with a median age of 2.8 y (range, 0.2–8.6 y). Most patients (26/34 [76.5%]) had advanced disease (stage 3 or 4). *MYCN* amplification was noted in 7 of 32 patients (21.9%) with available data. Among the 34 patients, 25 had 1 tumor, 7 had 2 tumors, 1 had 3 tumors, and 1 had 7 tumors (because of multiple relapses). Tumors from the same patients were sampled at different surgical times. The histologic types of the 50 tumors included 26 neuroblastomas (52%), 11 ganglioneuroblastomas (22%), 5 ganglioneuromas (10%), and 8 lesions without viable tumor cells (16%). Most tumors (33/50 [66%]) were in the abdomen. Details on the clinical features of patients and tumors are listed in Table 1.

Characteristics of ^{18}F-FDOPA PET in Neuroblastic Tumors

In patients with no evidence of disease, ^{18}F-FDOPA uptake was noted over the basal ganglia, gallbladder, kidneys, urinary tract, and epiphyseal plates of the long bones (Fig. 1). The basal ganglia, which contain dopaminergic neurons with AADC activity, may serve as an internal positive control. Forty-two (84%) tumors were avid on ^{18}F-FDOPA PET scans. In patients with active disease, ^{18}F-FDOPA PET clearly visualized the primary tumor (Fig. 2A, middle panel) and probable metastatic sites such as lymph nodes, bone or bone marrow, skull, and brain (Supplemental Fig. 1; supplemental materials are available online only at http://jnm.snmjournals.org).

^{18}F-FDOPA PET successfully detected 41 of the 42 neuroblastic tumors with viable tumor cells, including 25 of 26 neuroblastomas, all 11 ganglioneuroblastomas, and all 5 ganglioneuromas, with a sensitivity of 97.6% (95% confidence interval, 87.4%–99.9%). The only false-negative image was for an adrenal tumor in a 5-y-old girl with stage 4, MYCN-amplified disease after induction chemotherapy. Histologic examination showed a focal neuroblastoma with treatment effects and scattered residual tumor cells. On the other hand, 7 of the 8 lesions without viable tumor cells were negative on ^{18}F-FDOPA PET with a specificity of 87.5% (47.3%–99.7%). The only ^{18}F-FDOPA false-positive image was for an adrenal tumor in a 3-y-old girl with stage

TABLE 1
Clinical Characteristics of Patients with Neuroblastic Tumors

Characteristic	*n*
Age (*n* = 34)	
Infant (<1 y)	7 (20.6)
Noninfant (≥1 y)	27 (79.4)
Sex (*n* = 34)	
Female	14 (41.2)
Male	20 (58.8)
Stage on International Neuroblastoma Staging System (*n* = 34)	
1	5 (14.7)
2	1 (2.9)
3	3 (8.8)
4	23 (67.7)
4S	2 (5.9)
MYCN status (*n* = 34)	
Amplified	7 (20.6)
Nonamplified	25 (73.5)
Unknown	2 (5.9)
Tumor site (*n* = 50)	
Adrenal	18 (36)
Retroperitoneum	15 (30)
Mediastinum	3 (6)
Liver	2 (4)
Lungs	3 (6)
Head	2 (4)
Spine	1 (2)
Limbs	5 (10)
Lymph node	1 (2)
Timing of surgery (*n* = 50)	
At diagnosis	19 (38)
During chemotherapy	18 (36)
On suspicion of relapse	13 (26)
Histology (*n* = 50)	
Neuroblastoma	26 (52)
Ganglioneuroblastoma	11 (22)
Ganglioneuroma	5 (10)
No viable tumor cells*	8 (16)
Urinary VMA (*n* = 50)	
Elevated	12 (24)
Nonelevated	36 (72)
Missing	2 (4)

*Including 1 fibrosis, 2 inflammation, 2 necrotic tissue, and 3 lesions with no evidence of residual malignancy.
Data in parentheses are percentages.

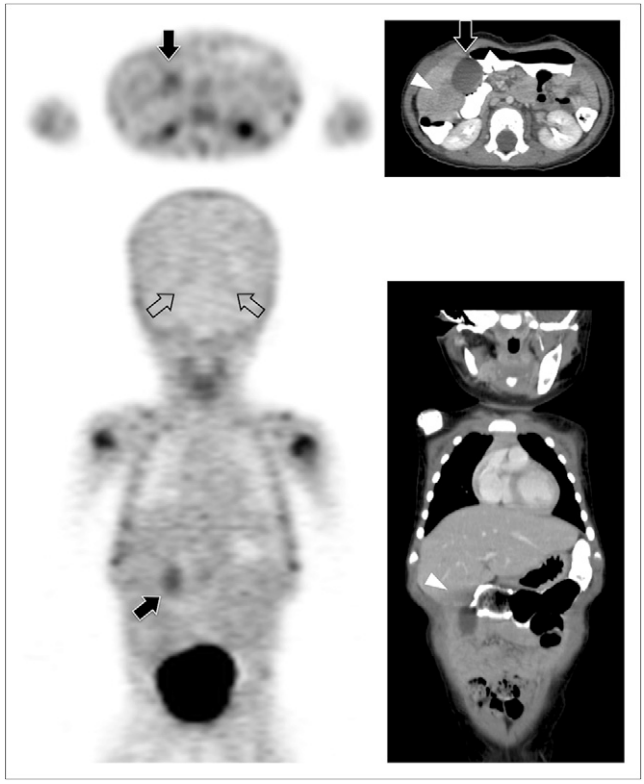

FIGURE 1. Normal ^{18}F-FDOPA uptake pattern. Representative transverse and coronal PET images (left) from 19-mo-old girl with stage 4S, *MYCN*-amplified disease after completion of therapy show normal uptake over basal ganglia (open arrows), gallbladder (solid arrows), urinary tract, and epiphyseal plates of long bones. Because of hypointense lesion over right inferior segment of liver on concomitant CT scan with contrast enhancement (arrowheads, right), mass was resected surgically, and it proved to be fibrosis only.

4 neuroblastoma after chemotherapy. The histology revealed no evidence of residual malignancy, but 2 ganglia were found in 1 section.

Comparison of ^{18}F-FDOPA PET, ^{123}I-MIBG Scan, and ^{18}F-FDG PET

In tumors that were studied with different modalities concomitantly, ^{18}F-FDOPA and ^{18}F-FDG PET demonstrated a higher resolution and tumor delineation than ^{123}I-MIBG scanning did (Fig. 2A). The sensitivity, specificity, and accuracy between ^{18}F-FDOPA PET and ^{123}I-MIBG scanning or ^{18}F-FDG PET are summarized in Table 2.

^{123}I-MIBG scintigraphy was performed concomitantly for 18 tumors with a sensitivity of 75% (47.6%–92.7%) and a specificity of 100% (15.8%–100%). Three of the four ^{123}I-MIBG–negative neuroblastic tumors were successfully detected by both ^{18}F-FDOPA and ^{18}F-FDG PET (Supplemental Fig. 2A), whereas the remaining ^{123}I-MIBG–negative neuroblastic tumor was visualized only by ^{18}F-FDOPA PET (Fig. 2B). The sensitivity of ^{123}I-MIBG scintigraphy was significantly lower than that of ^{18}F-FDOPA PET (75% [12/16] vs. 100% [16/16], P = 0.0455), and the specificity between these 2 modalities was not significantly different (100% [2/2] vs. 50% [1/2], P = 0.3173).

^{18}F-FDG PET was performed concomitantly for 46 tumors with a sensitivity of 86.8% (71.9%–95.6%) and a specificity of 62.5% (24.5%–91.5%). Four of the five ^{18}F-FDG false-negative tumors were successfully detected by ^{18}F-FDOPA PET (Supplemental Fig. 2B, except for the aforementioned ^{18}F-FDOPA false-negative tumor), whereas two of the three ^{18}F-FDG false-positive tumors remained true-negative on ^{18}F-FDOPA PET (except for the aforemen-

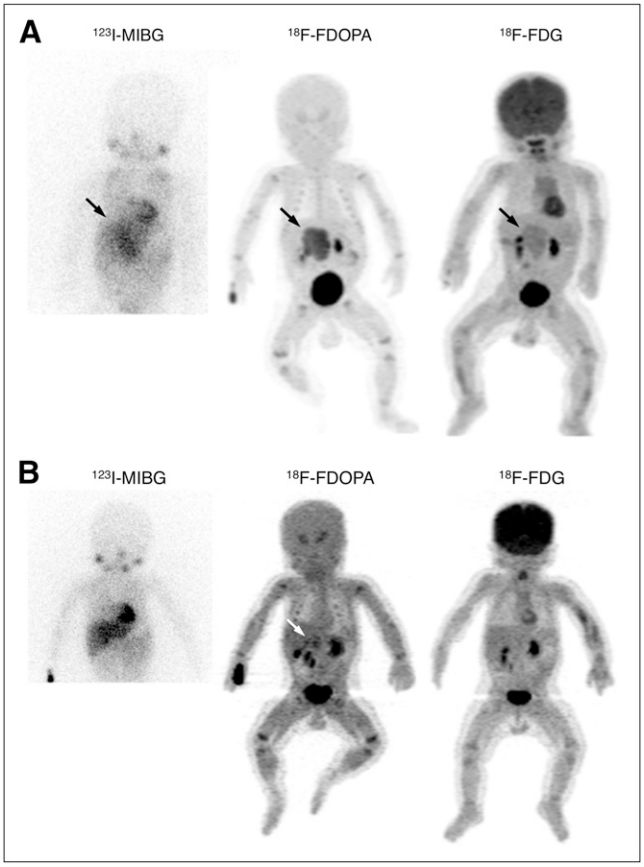

FIGURE 2. Comparison among ^{123}I-MIBG, ^{18}F-FDOPA PET, and ^{18}F-FDG PET images. (A) A 3-mo-old boy with stage 3, MYCN-nonamplified disease at diagnosis shows ^{123}I-MIBG-positive, ^{8}F-FDOPA-positive, and ^{8}F-FDG-positive findings. Histology of right adrenal tumor showed poorly differentiated neuroblastoma. (B) After 3 courses of chemotherapy, imaging results become ^{123}I-MIBG–negative, ^{8}F-FDOPA–positive, and ^{8}F-FDG–negative before total resection of tumor. Histology confirmed presence of neuroblastic cells.

tioned ^{18}F-FDOPA false-positive tumor). The sensitivity of ^{18}F-FDG PET was significantly lower than that of ^{18}F-FDOPA PET (86.8% [33/38] vs. 97.4% [37/38], P = 0.0455), whereas the specificity of ^{18}F-FDG PET tended to be lower than that of ^{18}F-FDOPA PET (62.5% [5/8] vs. 87.5% [7/8], P = 0.1573). On receiver-operating-characteristic analysis, the area under the curve for ^{18}F-FDG PET was marginally smaller than that for ^{18}F-FDOPA PET (n = 45; area under the curve, 0.8801 vs. 0.9645, P = 0.0682; Supplemental Fig. 3).

Among 17 tumors with triplet images, ^{123}I-MIBG–positive tumors (n = 11) showed significantly higher ^{18}F-FDOPA uptake (median SUV_{max}, 5.584 vs. 2.634, P = 0.0348; median tumor-to-liver uptake ratio, 3.195 vs. 1.623, P = 0.027) and urinary VMA (median level, 3.40 vs. 1.16 mg/d, P = 0.0181) than did the ^{123}I-MIBG–negative tumors, whereas there was no significant difference in their ^{18}F-FDG uptake (median SUV_{max}, 3.316 vs. 1.834, P = 0.107; median tumor-to-liver uptake ratio, 2.170 vs. 1.255,

TABLE 2
Sensitivity and Specificity of ^{18}F-FDOPA PET in Comparison to ^{123}I-MIBG or ^{18}F-FDG PET Imaging

Modality	Sensitivity	Specificity	Accuracy	Area under curve*
All tissue-proven tumors (n = 50, including 42 with viable tumor cells)				
^{18}F-FDOPA PET	41/42 (97.6%; 95%CI, 87.4–99.9)	7/8 (87.5%; 95%CI, 47.3–99.7)	48/50 (96.0%)	0.9680 (95%CI, 0.9193–1.0000)†
Tumors with concomitant ^{123}I-MIBG scanning (n = 18, including 16 with viable tumor cells)				
^{18}F-FDOPA PET	16/16 (100.0%; 95%CI, 79.4–100.0)	1/2 (50.0%; 95%CI, 1.26–98.7)	17/18 (94.4%)	0.9062 (95%CI, 0.6976–1.0000)
^{123}I-MIBG scanning	12/16 (75.0%; 95%CI, 47.6–92.7)	2/2 (100.0%; 95%CI, 15.8–100.0)	14/18 (77.8%)	Nonapplicable
P	0.0455	0.3173		Nonapplicable
Tumors with concomitant ^{18}F-FDG PET (n = 46, including 38 with viable tumor cells)				
^{18}F-FDOPA PET	37/38 (97.4%; 95%CI, 86.2–99.9)	7/8 (87.5%; 95%CI, 47.3–99.7)	44/46 (95.6%)	0.9645 (95%CI, 0.9101–1.000)†
^{18}F-FDG PET	33/38 (86.8%; 95%CI, 71.9–95.6)	5/8 (62.5%; 95%CI, 24.5–91.5)	38/46 (82.6%)	0.8801 (95%CI, 0.7861–0.9740)†
P	0.0455	0.1573		0.0682

*Calculated from tumor-to-liver SUV ratio in PET studies.
†Excluding 1 infant with diffuse hepatic uptake at diagnosis, which precluded calculation of tumor-to-liver uptake ratio.

$P = 0.2677$) (Fig. 3). Analysis of the performance of individual imaging methods among these triplets is presented in the supplemental results.

^{18}F-FDOPA Uptake, AADC Gene Expression, and Urinary VMA Excretion

In 15 nonhepatic tumors, the median AADC gene expression level was 6.898×10^{-3} (interquartile range, 2.109–27.58 $\times$ 10^{-3}), whereas their median SUV_{max} was 2.846 (interquartile range, 2.406–4.996), and their median tumor-to-liver uptake ratio was 2.070 (interquartile range, 1.895–3.465). There was a strong correlation between AADC gene expression and ^{18}F-FDOPA uptake (SUV_{max}, Spearman $\rho = 0.8179$, $P = 0.0002$; tumor-to-liver uptake ratio, $\rho = 0.8929$, $P < 0.0001$; Fig. 4A), and tumors with stronger ^{18}F-FDOPA uptake (tumor-to-liver uptake ratio $\geq$ 2) expressed significantly higher levels of AADC messenger RNA ($P = 0.0143$; Fig. 4B). In 47 tumors with a concomitant urinary VMA result, a significant correlation between VMA and ^{18}F-FDOPA uptake was also observed (supplemental results and Supplemental Fig. 4). These results suggested that in neuroblastic tumors, higher uptake of ^{18}F-FDOPA reflected not only higher levels of AADC expression but also more active downstream catecholamine metabolism.

DISCUSSION

This study demonstrated the feasibility, characteristics, clinical utility, and molecular basis of ^{18}F-FDOPA PET in neuroblastic tumors. ^{18}F-FDOPA PET was well tolerated in children with neuroblastic tumors. The 90-min interval between ^{18}F-FDOPA injection and PET scanning was much shorter than the standard 24-h interval for ^{123}I-MIBG scans (*26*) and allowed a single visit of the patient. ^{18}F-FDOPA PET clearly visualized primary and metastatic neuroblastic tumors (Fig. 2 and Supplemental Fig. 1) and detected all histologic types of neuroblastic tumors at a sensitivity of 97.6% and a specificity of 87.5% (Table 2). Because all four ^{123}I-MIBG false-negative neuroblastic tumors were successfully visualized by ^{18}F-FDOPA PET, including a patient whose tumor was detected by ^{18}F-FDOPA but not by ^{18}F-FDG (Fig. 2B), our findings suggest the complementary role of ^{18}F-FDOPA PET in detecting neuroblastic tumors in addition to traditional ^{123}I-MIBG and ^{18}F-FDG scans. However, because the number of patients was limited and ^{123}I-MIBG scanning was performed in only some of them, we stress that ^{123}I-/^{131}I-MIBG scans are still mandatory for neuroblastic tumors (*27*). In particular, when incorporation of ^{131}I-MIBG therapy is under consideration as part of multimodality therapy for high-risk disease, positive results on ^{123}I-/^{131}I-MIBG scanning should be a prelude (*28*).

Although ^{18}F-FDOPA PET has been used for striatal imaging in parkinsonism since the 1980s, its application to tumor imaging, especially in neuroendocrine tumors, is promising (*6,7*). For example, in head and neck paragangliomas, ^{18}F-FDOPA PET has been proven more efficacious than ^{18}F-fluorodopamine PET, ^{18}F-FDG PET, ^{123}I-MIBG scintigraphy, or ^{111}In-pentetreotide scintigraphy (*29*). Because neuroblastic tumors predominate in young children, physiologic uptake of ^{18}F-FDOPA was shown in the basal ganglia, epiph-

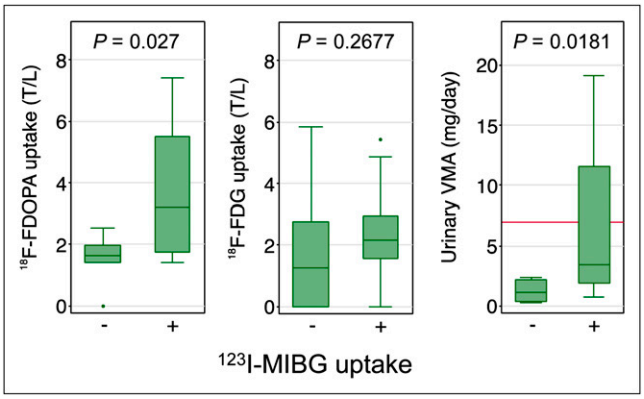

FIGURE 3. Comparison of ^{18}F-FDOPA uptake, ^{18}F-FDG uptake, and urinary VMA by ^{123}I-MIBG avidity among 17 tumors with concomitant results (reference line, upper limit of VMA).

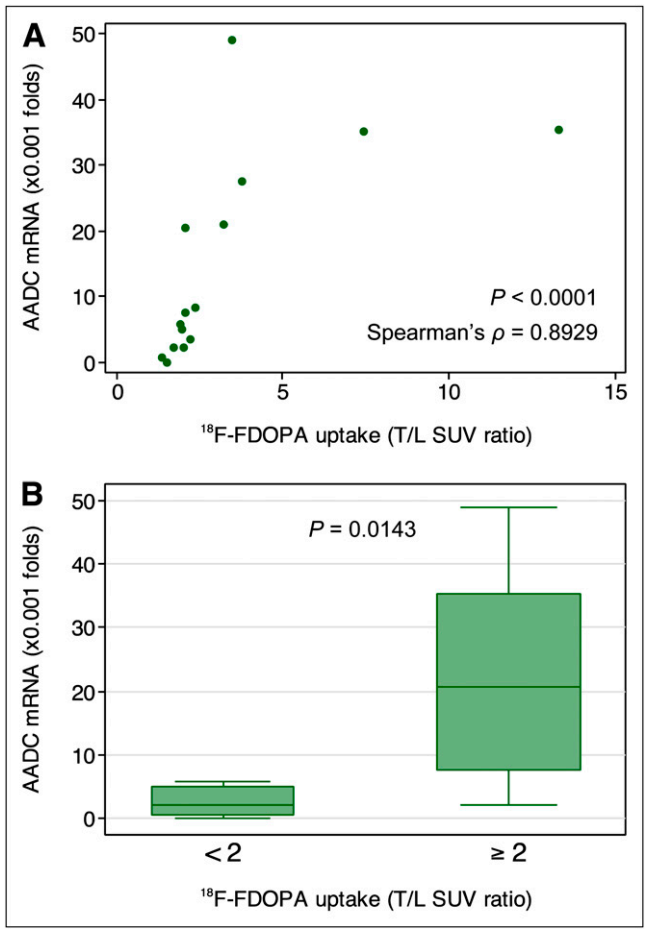

FIGURE 4. Relationship between tumor uptake of ^{18}F-FDOPA and AADC expression ($n = 15$ nonhepatic tumors). mRNA = messenger RNA; T/L = tumor-to-liver uptake ratio.

yseal plates of the long bones, kidneys, and liver and gastrointestinal tract (at lower intensity) in concordance with the tissue distribution of AADC transcripts (*30*), and also in the urinary tract and gallbladder, where catecholamine metabolites are excreted (Fig. 1). Because neuroblastic tumors are frequently located in the retroperitoneum, focal high uptake in the gallbladder and ureters should be carefully compared with anatomic images of CT or ultrasound in equivocal cases, as has been recommended in neuroendocrine tumors (*6*). In addition, the moderate uptake of ^{18}F-FDOPA by the liver can also mask neuroblastic tumors that have metastasized to the liver. Despite these potential limitations, we observed minimal background uptake of ^{18}F-FDOPA in sites that are commonly involved with primary or metastatic neuroblastic tumors, including the adrenal glands, paraspinal ganglia, skull and brain, lymph nodes, and bone or bone marrow (except for the epiphyseal plates), thereby providing a clear contrast in detecting neuroblastic tumors.

Because the enzymatic target of ^{18}F-FDOPA is AADC, the presence of AADC activity in neuroblastic cells provides the molecular basis of this study (*12*). AADC was expressed in 100% of neuroblastic tumors and 0% of other common pediatric tumors (*31*), serving as a sensitive and specific biomarker of neuroblastic tumors. In cells derived from the sympathetic nervous system, AADC converts L-DOPA to dopamine, which is subsequently converted to norepinephrine and epinephrine (*3,10*). These catecholamines are then metabolized into homovanillic acid and VMA and excreted in the urine (*9,32*). We showed that ^{18}F-FDOPA uptake in neuroblastic tumors significantly correlated with not only AADC expression (Fig. 4) but also urinary VMA levels (Supplemental Fig. 4). Therefore, the biologic activity of neuroblastic cells in vivo, in terms of catecholamine biosynthesis, could be vividly reflected by the noninvasive ^{18}F-FDOPA PET study. Given that AADC expression (*33–35*) and urinary VMA (*32*) have been found to be associated with neuroblastic tumor patients' prognosis, the signal intensity of neuroblastic tumors on ^{18}F-FDOPA PET might also confer prognostic implications and require further investigations.

The current standard imaging studies for the staging and follow-up of neuroblastic tumors include CT/MR imaging and ^{123}I-MIBG scintigraphy (*36*). CT and MR imaging depict the anatomic extent of neuroblastic tumors, but they do not functionally characterize the lesions, as 7 of 8 lesions detected by CT/MR imaging showed negative uptake on ^{18}F-FDOPA PET with no viable tumor cells on histopathology (Fig. 1; Table 2). On the other hand, ^{123}I-MIBG targets norepinephrine transporter and specifically localizes neuroblastic tumors. We observed a strong relationship between ^{123}I-MIBG avidity and ^{18}F-FDOPA uptake or urinary VMA (Fig. 3), consistent with microarray studies showing that the adrenergic genes were collectively and differentially expressed in the same direction among neuroblastic tumors (*33–35*).

^{18}F-FDG PET, another commonly used functional scan for neuroblastic tumors, has a relatively high sensitivity and good image quality for detecting neuroblastic tumors. However, because ^{18}F-FDG is taken up by cells with a high glucose metabolic rate, ^{18}F-FDG imaging of neuroblastic tumor could be confounded by physiologic signals in the brain (Fig. 2), sites with inflammation of nonmalignant causes, and bone marrow undergoing normal hyperplasia after myelosuppressive chemotherapy (*37–39*). In comparison to ^{18}F-FDG PET, ^{18}F-FDOPA PET provided a better contrast for cranial or brain lesions (Supplemental Fig. 1B) and a higher sensitivity in detecting neuroblastic tumors (Table 2). Interestingly, it has been shown in pulmonary neuroendocrine tumors that typical carcinoids have significantly higher uptake of ^{68}Ga-DOTATATE and less uptake of ^{18}F-FDG than do tumors of higher grade (*40*), thereby raising the probability that in neuroblastic tumors, ^{18}F-FDG and ^{18}F-FDOPA PET might also complement each other by targeting distinct biologic pathways.

CONCLUSION

In this preliminary study with a small cohort of patients, ^{18}F-FDOPA PET exhibited a high sensitivity and specificity of 97.6% and 87.5%, respectively, in detecting neuroblastic tumors with viable tumor cells. ^{18}F-FDOPA has detected 4 of 4 neuroblastic tumors false-negative on ^{123}I-MIBG and 4 of 5 false-negative on ^{18}F-FDG, suggesting its complementary role to current ^{123}I-MIBG scintigraphy and ^{18}F-FDG PET scans. Because ^{18}F-FDOPA uptake in neuroblastic tumors significantly correlated with AADC expression and urinary VMA excretion, ^{18}F-FDOPA PET could potentially serve as a noninvasive functional imaging method in detecting viable neuroblastic cells. Further studies with larger patient cohorts comprehensively comparing various imaging methods are required to validate the clinical usefulness of ^{18}F-FDOPA PET in the assessment of neuroblastic tumors.

DISCLOSURE

The costs of publication of this article were defrayed in part by the payment of page charges. Therefore, and solely to indicate this fact, this article is hereby marked "advertisement" in accordance with 18 USC section 1734. This study was supported by National Science Council, Taiwan (grants NSC 96-NU-7-002-005 and NSC 100-NU-E-002-004). No other potential conflict of interest relevant to this article was reported.

ACKNOWLEDGMENTS

We thank Ms. Hsiao-Ling Chen and Chia-Hsuan Yang at the Department of Nursing, College of Medicine, National Taiwan University, Taipei, Taiwan, for coordinating a patient- and family-centered support group that has provided

consistent help in patient enrollment and communication throughout the study period. We also thank collaborators of the NTU Neuroblastoma Study Group, including Drs. Fon-Jou Hsieh, Hong-Shiee Lai, Steven Shinn-Forng Peng (National Taiwan University Hospital, Taipei, Taiwan), Min-Chuan Huang, Hsueh-Fen Juan (National Taiwan University, Taipei, Taiwan), Yeou-Guang Tsay (National Yang-Ming University, Taipei, Taiwan), and Christina Ling Chang (National Cheng Kung University, Tainan, Taiwan), for their contribution to the design of this study. This study was presented in part at the 57th annual meeting of the Society of Nuclear Medicine, Salt Lake City, Utah, June 5–9, 2010; at the 14th Advances in Neuroblastoma Research Meeting, Stockholm, Sweden, June 21–24, 2010; and at the 58th annual meeting of the Society of Nuclear Medicine, San Antonio, Texas, June 4–8, 2011.

REFERENCES

1. Grovas A, Fremgen A, Rauck A, et al. The National Cancer Data Base report on patterns of childhood cancers in the United States. *Cancer.* 1997;80:2321–2332.
2. Hoehner JC, Gestblom C, Hedborg F, Sandstedt B, Olsen L, Pahlman S. A developmental model of neuroblastoma: differentiating stroma-poor tumors' progress along an extra-adrenal chromaffin lineage. *Lab Invest.* 1996;75:659–675.
3. Ilias I, Shulkin B, Pacak K. New functional imaging modalities for chromaffin tumors, neuroblastomas and ganglioneuromas. *Trends Endocrinol Metab.* 2005;16:66–72.
4. DuBois SG, Kalika Y, Lukens JN, et al. Metastatic sites in stage IV and IVS neuroblastoma correlate with age, tumor biology, and survival. *J Pediatr Hematol Oncol.* 1999;21:181–189.
5. Kushner BH. Neuroblastoma: a disease requiring a multitude of imaging studies. *J Nucl Med.* 2004;45:1172–1188.
6. Jager PL, Chirakal R, Marriott CJ, Brouwers AH, Koopmans KP, Gulenchyn KY. 6-L-^{18}F-fluorodihydroxyphenylalanine PET in neuroendocrine tumors: basic aspects and emerging clinical applications. *J Nucl Med.* 2008;49:573–586.
7. Minn H, Kauhanen S, Seppanen M, Nuutila P. ^{18}F-FDOPA: a multiple-target molecule. *J Nucl Med.* 2009;50:1915–1918.
8. Yee RE, Huang SC, Togasaki DM, Langston JW, Satyamurthy N, Barrio JR. Imaging and therapeutics: the role of neuronal transport in the regional specificity of L-DOPA accumulation in brain. *Mol Imaging Biol.* 2002;4:208–218.
9. Kumakura Y, Cumming P. PET studies of cerebral levodopa metabolism: a review of clinical findings and modeling approaches. *Neuroscientist.* 2009;15:635–650.
10. Koopmans KP, Neels ON, Kema IP, et al. Molecular imaging in neuroendocrine tumors: molecular uptake mechanisms and clinical results. *Crit Rev Oncol Hematol.* 2009;71:199–213.
11. Neels OC, Koopmans KP, Jager PL, et al. Manipulation of [^{11}C]-5-hydroxytryptophan and 6-[^{18}F]fluoro-3,4-dihydroxy-L-phenylalanine accumulation in neuroendocrine tumor cells. *Cancer Res.* 2008;68:7183–7190.
12. Gazdar AF, Helman LJ, Israel MA, et al. Expression of neuroendocrine cell markers L-dopa decarboxylase, chromogranin A, and dense core granules in human tumors of endocrine and nonendocrine origin. *Cancer Res.* 1988;48:4078–4082.
13. Shimada H, Ambros IM, Dehner LP, et al. The International Neuroblastoma Pathology Classification (the Shimada system). *Cancer.* 1999;86:364–372.
14. Tsai HY, Hsi BL, Hung IJ, et al. Correlation of MYCN amplification with MCM7 protein expression in neuroblastomas: a chromogenic in situ hybridization study in paraffin sections. *Hum Pathol.* 2004;35:1397–1403.
15. Brodeur GM, Pritchard J, Berthold F, et al. Revisions of the international criteria for neuroblastoma diagnosis, staging, and response to treatment. *J Clin Oncol.* 1993;11:1466–1477.
16. Chang HH, Lee H, Hu MK, et al. Notch1 expression predicts an unfavorable prognosis and serves as a therapeutic target of patients with neuroblastoma. *Clin Cancer Res.* 2010;16:4411–4420.
17. Hsu WM, Jen YM, Lee H, et al. The influence of biologic factors on the surgical decision in advanced neuroblastoma. *Ann Surg Oncol.* 2006;13:238–244.
18. de Vries EFJ, Luurtsema G, Brüssermann M, Elsinga PH, Vaalburg W. Fully automated synthesis module for the high yield one-pot preparation of 6-[^{18}F]fluoro-L-DOPA. *Appl Radiat Isot.* 1999;51:389–394.
19. Timmers HJ, Hadi M, Carrasquillo JA, et al. The effects of carbidopa on uptake of 6-^{18}F-fluoro-L-DOPA in PET of pheochromocytoma and extraadrenal abdominal paraganglioma. *J Nucl Med.* 2007;48:1599–1606.
20. Ishikawa T, Dhawan V, Chaly T, et al. Fluorodopa positron emission tomography with an inhibitor of catechol-O-methyltransferase: effect of the plasma 3-O-methyldopa fraction on data analysis. *J Cereb Blood Flow Metab.* 1996;16:854–863.
21. Orlefors H, Sundin A, Lu L, et al. Carbidopa pretreatment improves image interpretation and visualisation of carcinoid tumours with ^{11}C-5-hydroxytryptophan positron emission tomography. *Eur J Nucl Med Mol Imaging.* 2006;33:60–65.
22. Yang AS, Chiang TC, Shen LH. Acute intravenous injection toxicity study of MIBG in mice. *Drug Chem Toxicol.* 2010;33:17–19.
23. Hsu WM, Hsieh FJ, Jeng YM, et al. Calreticulin expression in neuroblastoma: a novel independent prognostic factor. *Ann Oncol.* 2005;16:314–321.
24. Chang YT, Mues G, Hyland K. Alternative splicing in the coding region of human aromatic L-amino acid decarboxylase mRNA. *Neurosci Lett.* 1996;202:157–160.
25. Avgeris M, Koutalellis G, Fragoulis EG, Scorilas A. Expression analysis and clinical utility of L-Dopa decarboxylase (DDC) in prostate cancer. *Clin Biochem.* 2008;41:1140–1149.
26. Olivier P, Colarinha P, Fettich J, et al. Guidelines for radioiodinated MIBG scintigraphy in children. *Eur J Nucl Med Mol Imaging.* 2003;30:B45–B50.
27. Naranjo A, Parisi MT, Shulkin BL, et al. Comparison of ^{123}I-metaiodobenzylguanidine (MIBG) and ^{131}I-MIBG semi-quantitative scores in predicting survival in patients with stage 4 neuroblastoma: a report from the Children's Oncology Group. *Pediatr Blood Cancer.* 2011;56:1041–1045.
28. Matthay KK, Yanik G, Messina J, et al. Phase II study on the effect of disease sites, age, and prior therapy on response to iodine-131-metaiodobenzylguanidine therapy in refractory neuroblastoma. *J Clin Oncol.* 2007;25:1054–1060.
29. King KS, Chen CC, Alexopoulos DK, et al. Functional imaging of SDHx-related head and neck paragangliomas: comparison of ^{18}F-fluorodihydroxyphenylalanine, ^{18}F-fluorodopamine, ^{18}F-fluoro-2-deoxy-D-glucose PET, ^{123}I-metaiodobenzylguanidine scintigraphy, and ^{111}In-pentetreotide scintigraphy. *J Clin Endocrinol Metab.* 2011;96:2779–2785.
30. O'Malley KL, Harmon S, Moffat M, Uhland-Smith A, Wong S. The human aromatic L-amino acid decarboxylase gene can be alternatively spliced to generate unique protein isoforms. *J Neurochem.* 1995;65:2409–2416.
31. Gilbert J, Haber M, Bordow SB, Marshall GM, Norris MD. Use of tumor-specific gene expression for the differential diagnosis of neuroblastoma from other pediatric small round-cell malignancies. *Am J Pathol.* 1999;155:17–21.
32. Nakagawara A, Ikeda K. N-myc oncogene amplification and catecholamine metabolism in children with neuroblastoma. *Lancet.* 1987;1(8572):559.
33. Wilzén A, Nilsson S, Sjoberg RM, Kogner P, Martinsson T, Abel F. The Phox2 pathway is differentially expressed in neuroblastoma tumors, but no mutations were found in the candidate tumor suppressor gene PHOX2A. *Int J Oncol.* 2009;34:697–705.
34. Gershon TR, Shirazi A, Qin LX, Gerald WL, Kenney AM, Cheung NK. Enteric neural crest differentiation in ganglioneuromas implicates Hedgehog signaling in peripheral neuroblastic tumor pathogenesis. *PLoS ONE.* 2009;4:e7491.
35. Bourdeaut F, Janoueix-Lerosey I, Lucchesi C, et al. Cholinergic switch associated with morphological differentiation in neuroblastoma. *J Pathol.* 2009;219:463–472.
36. Monclair T, Brodeur GM, Ambros PF, et al. The International Neuroblastoma Risk Group (INRG) staging system: an INRG Task Force report. *J Clin Oncol.* 2009;27:298–303.
37. Kushner BH, Yeung HW, Larson SM, Kramer K, Cheung NK. Extending positron emission tomography scan utility to high-risk neuroblastoma: fluorine-18 fluorodeoxyglucose positron emission tomography as sole imaging modality in follow-up of patients. *J Clin Oncol.* 2001;19:3397–3405.
38. Taggart DR, Han MM, Quach A, et al. Comparison of iodine-123 metaiodobenzylguanidine (MIBG) scan and [^{18}F]fluorodeoxyglucose positron emission tomography to evaluate response after iodine-131 MIBG therapy for relapsed neuroblastoma. *J Clin Oncol.* 2009;27:5343–5349.
39. Sharp SE, Shulkin BL, Gelfand MJ, Salisbury S, Furman WL. ^{123}I-MIBG scintigraphy and ^{18}F-FDG PET in neuroblastoma. *J Nucl Med.* 2009;50:1237–1243.
40. Kayani I, Conry BG, Groves AM, et al. A comparison of ^{68}Ga-DOTATATE and ^{18}F-FDG PET/CT in pulmonary neuroendocrine tumors. *J Nucl Med.* 2009;50:1927–1932.

JNM The Journal of NUCLEAR MEDICINE

Characterization of Neuroblastic Tumors Using ^{18}F-FDOPA PET

Meng-Yao Lu, Yen-Lin Liu, Hsiu-Hao Chang, Shiann-Tarng Jou, Yung-Li Yang, Kai-Hsin Lin, Dong-Tsamn Lin, Ya-Ling Lee, Hsinyu Lee, Pei-Yi Wu, Tsai-Yueh Luo, Lie-Hang Shen, Shiu-Feng Huang, Yung-Feng Liao, Wen-Ming Hsu and Kai-Yuan Tzen

J Nucl Med. 2013;54:42-49.
Published online: December 4, 2012.
Doi: 10.2967/jnumed.112.102772

The Journal of Nuclear Medicine is published monthly.
SNMMI | Society of Nuclear Medicine and Molecular Imaging
1850 Samuel Morse Drive, Reston, VA 20190.
(Print ISSN: 0161-5505, Online ISSN: 2159-662X)

SNMMI SOCIETY OF NUCLEAR MEDICINE AND MOLECULAR IMAGING